Rotational behavior of ^{120,122,124}Te

M. Saxena,[1] R. Kumar,[2] A. Jhingan,[2] S. Mandal,[1] A. Stolarz,[3] A. Banerjee,[1] R. K. Bhowmik,[2] S. Dutt,[4] J. Kaur,[5] V. Kumar,[6] M. Modou Mbaye,[7] V. R. Sharma,[8] and H.-J. Wollersheim[9]

[1]*Department of Physics & Astrophysics, University of Delhi, Delhi 110007, India*
[2]*Inter-University Accelerator Centre, New Delhi 110067, India*
[3]*Heavy Ion Laboratory, University of Warsaw, Pasteura 5a, 02-093 Warsaw, Poland*
[4]*Department of Physics, Bareilly College, India*
[5]*Department of Physics, Panjab University, Chandigarh 160014, India*
[6]*Department of Physics, SLIET, Sangru 148106, India*
[7]*Cheikh Anta Diop University, Senegal*
[8]*Acc Lab, Department of Physics, A.M. University, Aligarh 202002, India*
[9]*GSI Helmholtzzentrum für Schwerionenforschung GmbH, D-64291 Darmstadt, Germany*

(Received 29 March 2014; revised manuscript received 23 June 2014; published 21 August 2014)

Three consecutive Coulomb excitation experiments were performed to measure the reduced transition probabilities in ^{120,122,124}Te by using a ^{58}Ni beam. For ^{120}Te the collectivity was remeasured with high precision yielding a $B(E2; 0^+_{\text{g.s.}} \rightarrow 2^+_1)$ value of 0.666 (20) e^{2}b^2. From the $B(E2)$ values connecting higher-lying states, the nuclear structure of ^{120,122,124}Te was determined and shows a rotational behavior quite in contrast with the vibrational structure of the level schemes. The data are compared with different models.

DOI: 10.1103/PhysRevC.90.024316 PACS number(s): 23.20.Js, 21.10.Re, 25.70.De, 27.60.+j

I. INTRODUCTION AND MOTIVATION

In semimagic nuclei, such as the tin isotopes, the seniority scheme [1] provides a very valuable tool for describing the low-energy spectra. In tellurium nuclei with two protons outside the major shell, the partial level schemes are dominated by the $1g_{7/2}$ orbit leading to 6^+ isomers in the vicinity of $N = 82$ shell closure. For the midshell nuclei ^{120,122,124}Te one observes the expected transition to vibrational-like structure with equal energy spacings between the phonon states which is depicted in Fig. 1.

This observation is in contrast to the measured quadrupole moments Q_{2^+} for the doubly even Te isotopes [3,4]. These quadrupole moments can reach 60% of that predicted by the symmetric rigid rotor. In the rotational model the following relation exists between the static quadrupole moment Q_{2^+} and the reduced transition probability $B(E2; 0^+_{\text{g.s.}} \rightarrow 2^+_1)$:

$$Q_{2^+} = -\frac{2}{7}\sqrt{\frac{16\pi}{5}B(E2; 0^+_{\text{g.s.}} \rightarrow 2^+_1)}$$

One aim of the present investigation is the remeasurement of the $B(E2; 0^+_{\text{g.s.}} \rightarrow 2^+_1)$ value in ^{120}Te with higher precision for a comparison with large-scale shell model (LSSM) [5] calculations. In addition the investigation of reduced transition probabilities connecting higher-lying states will shed light on the nuclear structure of ^{120,122,124}Te. In the past, different models, such as the interacting boson approximation (IBA) [6], the general collective model [7], and particle-core coupling model [8,9] have been used to examine the limited experimental results in ^{120}Te [10]. In the next section experimental details of the Coulomb excitation experiment will be discussed while the data analysis is described in Sec. III. The experimental results are compared with microscopic calculations and different collective models in Sec. IV.

II. EXPERIMENTAL DETAILS

The experiment was performed at the Inter University Accelerator Centre (IUAC) in Delhi using a ^{58}Ni beam at 175 MeV to Coulomb excite three targets of ^{120}Te, ^{122}Te, and ^{124}Te, respectively. The beam energy was well below the safe bombarding energy (211 MeV) to ensure a pure electromagnetic interaction between the interacting particles. All targets were ∼0.150(5) mg/cm^2 thick with a thin carbon backing of 25–30 μg/cm^2. The thickness of both backing and deposited material was determined by a comparison between the measured energy loss of alpha particles with Stopping and Range of Ions in Matter (SRIM) [11] calculations. The isotopic enrichment for the ^{120}Te target was certified by the manufacturer to be 57.6% with the largest impurity contribution of ∼42% for ^{122}Te. The other two targets, ^{122}Te and ^{124}Te, were produced with highly enriched (∼99%) material.

Similar to our previous measurement [12], an annular gas-filled parallel-plate avalanche counter (PPAC) was placed 11 cm downstream of the target to detect both the scattered projectiles as well as the recoiling target nuclei in an angular range of $15^\circ \leqslant \vartheta_{\text{lab}} \leqslant 45^\circ$. The PPAC consisted of an anode foil, subdivided into 20 radial segments for the azimuthal angle φ_{lab} information, and a cathode plate of 50 concentric rings connected by an electronic delay line with 2 ns time-delay steps. The polar angle ϑ_{lab} was deduced by the delay-line differences between signals coming from the innermost and outermost ring. Deexcitation γ-rays emitted after Coulomb excitation were measured with four clover (Ge) detectors mounted at $\vartheta_\gamma \sim 135^\circ$ with respect to the beam direction. The φ_γ angles for the clover detectors were $\pm 55^\circ$ and $\pm 125^\circ$ with respect to the vertical direction. Individual energies and timing signals of the 16 Ge crystals of the four clover detectors were recorded in coincidence with the PPAC anode and cathode signals event by event. To avoid any systematic error, the

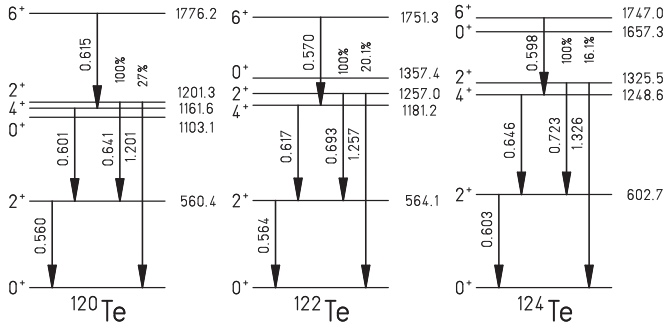

FIG. 1. Partial level schemes of ^{120,122,124}Te isotopes [2].

^{120}Te and ^{122}Te targets were used in turn every three hours for a total measuring time of approximately 50 hours. Energy and relative-efficiency calibrations were carried out by using a ^{152}Eu source.

III. DATA ANALYSIS AND RESULT

In the present experiment only one of the two reaction partners were detected in the PPAC. From the scattering angle (ϑ_p,φ_p) and the position of the Ge crystal $(\vartheta_\gamma,\varphi_\gamma)$, the Doppler-shift correction for the measured γ-ray energy was performed event by event. Typical Doppler-shift corrected γ-ray spectra for the systems $^{120}\text{Te} + {}^{58}\text{Ni}$ (solid line) and $^{122}\text{Te} + {}^{58}\text{Ni}$ (dashed line) are shown in Fig. 2. The displayed energy region shows the $2_1^+ \rightarrow 0_{\text{g.s.}}^+$ transition for distant collisions (assumption:^{58}Ni detected in PPAC), while the broad distribution on the left-hand side results from the wrongly corrected events for close collisions (Te detected in PPAC). It is very astonishing that one obtains the same γ-ray energy resolution of 4 keV in both systems. The expected ^{122}Te target impurity for the system $^{120}\text{Te} + {}^{58}\text{Ni}$ is not visible which

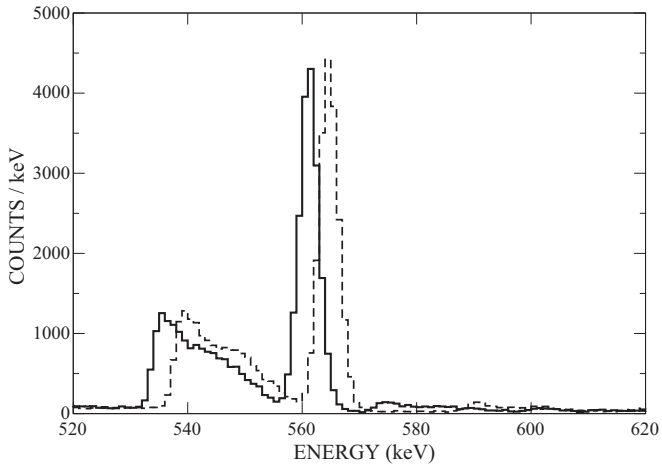

FIG. 2. Doppler-shift corrected γ-ray spectra for the $2_1^+ \rightarrow 0_{\text{g.s.}}^+$ transition measured for the system $^{120}\text{Te} + {}^{58}\text{Ni}$ (solid line) and $^{122}\text{Te} + {}^{58}\text{Ni}$ (dashed line) assuming ^{58}Ni being detected in the PPAC. The broad distribution on the left-hand side results from close collisions events, when Te recoils are detected in PPAC. A γ-ray energy resolution of 4 keV was obtained in both the systems.

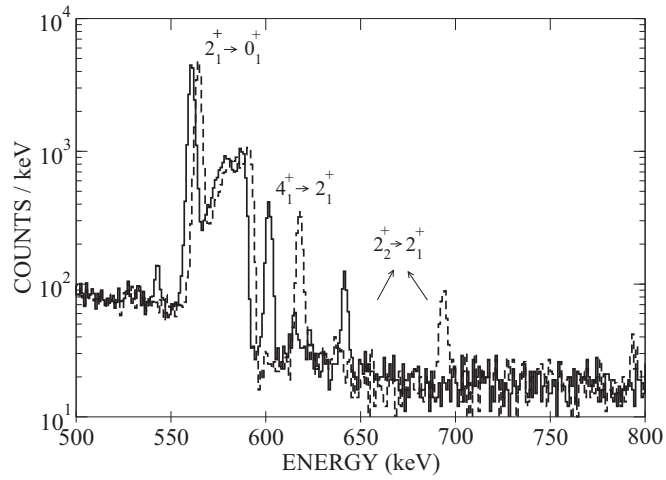

FIG. 3. Doppler-shift corrected γ-ray spectra for $^{120}\text{Te} + {}^{58}\text{Ni}$ (solid line) and $^{122}\text{Te} + {}^{58}\text{Ni}$ (dashed line) assuming Te being detected in the PPAC. The broad distribution on the right-hand side of the $2_1^+ \rightarrow 0_{\text{g.s.}}^+$ transition results from distant collision events, when ^{58}Ni nuclei are detected in PPAC.

should lead to double-hump structure (560 keV, 564 keV) with a total width of 7 keV.

Figure 3 shows Doppler-corrected γ-ray spectra for the systems $^{120}\text{Te} + {}^{58}\text{Ni}$ (solid line) and $^{122}\text{Te} + {}^{58}\text{Ni}$ (dashed line) assuming Te recoils being detected in the PPAC. Besides the $2_1^+ \rightarrow 0_{\text{g.s.}}^+$ transition, one observes additional transitions from the decay of higher-lying states. The expected target decomposition is also not visible, although the transitions in ^{120}Te and ^{122}Te are much better resolved, e.g., the $2_2^+ \rightarrow 2_1^+$ transition. We therefore concluded that the target enrichment for ^{120}Te is much higher than stated by the manufacturer (57.6%). From the γ-ray intensity of the $2_2^+ \rightarrow 2_1^+$ transition at 641 keV and the corresponding background intensity at 693 keV (expected $2_2^+ \rightarrow 2_1^+$ transition in ^{122}Te) measured for the $^{120}\text{Te} + {}^{58}\text{Ni}$ system and the analysis of the $^{122}\text{Te} + {}^{58}\text{Ni}$ system, we estimated the ^{120}Te target enrichment of 95.5% with an uncertainty of 2%. This measured target enrichment was considered for the analysis of the $B(E2; 0_{\text{g.s.}}^+ \rightarrow 2_1^+)$ value.

The excitation strength of the 2^+ state in ^{120}Te, ^{122}Te, and ^{124}Te were determined for distant collisions, with the first excited 2^+ state in ^{58}Ni used for normalization. It is important to note that the ^{58}Ni beam excitation on the carbon backing was not measured because of the limited angular range of the PPAC ($\vartheta_{\text{max}} = 11.9^\circ$). To obtain the $B(E2;\ 0_{\text{g.s.}}^+ \rightarrow 2_1^+)$ value in ^{120}Te, the experimental γ-ray intensity double ratio $[I_\gamma(^{120}\text{Te})/I_\gamma(^{58}\text{Ni})]/[I_\gamma(^{122}\text{Te})/I_\gamma(^{58}\text{Ni})]$ of the $2_1^+ \rightarrow 0_{\text{g.s.}}^+$ decays was determined (for details see Ref. [12]). This double ratio was corrected for the different Ge detector efficiency (uncertainty 1.7%) and target enrichments (1.5%). The theoretical cross sections were calculated for a set of $E2$ matrix elements with the Winther–de Boer Coulomb excitation code [13]. In these calculations the slowing down of the projectiles in the targets (0.5%), the uncertainty of the PPAC boundaries (0.3%) and the reference $B(E2; 0_{\text{g.s.}}^+ \rightarrow 2_1^+) = 0.660\,(6)$

TABLE I. Influence of the reorientation effect, hexadecapole moment, and matrix elements to higher-excited states on the $2_1^+ \rightarrow 0_{g.s.}^+ \gamma$-ray yield for distant collisions.

Reorientation effect	1%
Hexadecapole moment	0.1%
Higher excited states	1.1%

e^2b^2 in ^{122}Te were considered. Since the adopted $B(E2\uparrow)$ value in ^{122}Te is an evaluation of ten different experimental results [14], it becomes a reliable and precise reference point. The subsequent γ-ray decay was calculated for the particle-γ angular correlation (0.5%) including the internal conversion, $E2/M1$ mixing ratios and the finite geometry of the Ge detectors. In addition, the contributions of the reorientation effect, hexadecapole moment, and matrix elements connecting higher-excited states were investigated (see Table I). The influence of the reorientation effect on the $2_1^+ \rightarrow 0_{g.s.}^+ \gamma$-ray yield was examined by using the rather precise static quadrupole moments Q_{2^+} of the first-excited state in ^{122,124}Te isotopes (see Table II). Theoretical predictions of Q_{2^+} [15] confirm almost constant values for ^{120,122,124}Te. In case of ^{120}Te an uncertainty of 30% was assumed. For the hexadecapole matrix element theoretical $B(E4; 4_1^+ \rightarrow 0_{g.s}^+) = 7$ single particle units (s.p.u.)[16] value was used, while the matrix elements connecting higher-excited states were either taken from known data [2] or determined from the analysis at close collisions.

The resulting $B(E2; 0_{g.s.}^+ \rightarrow 2_1^+)$ value of 0.666 (20) e^2b^2 in ^{120}Te was adjusted in the Coulomb excitation calculations to reproduce the experimental double ratio. The reduced transition probabilities connecting higher-excited states were extracted for close collisions from the measured γ-ray yields normalized to the $2_1^+ \rightarrow 0_{g.s.}^+$ transition in the respective Te isotopes.

IV. DISCUSSION

In the following the collective strength of the measured reduced transition probabilities $B(E2; 0_{g.s.}^+ \rightarrow 2_1^+)$ are compared with neighboring nuclei and with predictions of large-scale shell model (LSSM) calculations.

If we compare the Te and Sn isotopic chains, we note that the collectivity in tellurium is two to three times larger than for the tin data. This can be understood in terms of two additional protons in Te above the $Z = 50$ shell closure. For ^{120}Te we obtain a Weisskopf estimate of 36 s.p.u., which corresponds to 12 s.p.u. for ^{118}Sn. The difference between two proton and two proton-hole configurations was investigated by plotting $B(E2; 0_{g.s.}^+ \rightarrow 2_1^+)$ values for tellurium and cadmium versus the neutron number (Fig. 4). Both distributions are almost identical, but they are asymmetric with respect to $N = 66$ midshell nuclei. The observed dependence on the element

TABLE II. Comparison of the measured data for the ^{120,122,124}Te isotopes with various available models.

	A	Experiment	Vibrator	Asymmetric rotor	IBA-2
$Q_s(2^+)/Q_0$	120		0	-0.179 $\gamma = 25^\circ$	-0.178
$Q_s(2^+)/Q_0$	122	-0.182 (12)		-0.105 $\gamma = 27.5^\circ$	-0.140
$Q_s(2^+)/Q_0$	124	-0.189 (16)			-0.066
$\frac{B(E2;4^+\rightarrow 2^+)}{B(E2;2^+\rightarrow 0^+)}$	120	1.640 (33)	2.0	1.426 $\gamma = 25^\circ$	1.514
$\frac{B(E2;4^+\rightarrow 2^+)}{B(E2;2^+\rightarrow 0^+)}$	122	1.500 (40)		1.394 $\gamma = 27.5^\circ$	1.470
$\frac{B(E2;4^+\rightarrow 2^+)}{B(E2;2^+\rightarrow 0^+)}$	124	1.162 (53)			1.456
$\frac{B(E2;6^+\rightarrow 4^+)}{B(E2;2^+\rightarrow 0^+)}$	120	2.37 (58)	3.0	1.781 $\gamma = 25^\circ$	1.82
$\frac{B(E2;6^+\rightarrow 4^+)}{B(E2;2^+\rightarrow 0^+)}$	122			1.748 $\gamma = 27.5^\circ$	1.710
$\frac{B(E2;6^+\rightarrow 4^+)}{B(E2;2^+\rightarrow 0^+)}$	124				1.614
$\frac{B(E2;2_2^+\rightarrow 2^+)}{B(E2;2^+\rightarrow 0^+)}$	120	1.215 (50)	2.0	0.906 $\gamma = 25^\circ$	1.560
$\frac{B(E2;2_2^+\rightarrow 2^+)}{B(E2;2^+\rightarrow 0^+)}$	122	0.954 (74)		1.255 $\gamma = 27.5^\circ$	1.525
$\frac{B(E2;2_2^+\rightarrow 2^+)}{B(E2;2^+\rightarrow 0^+)}$	124	1.115 (175)			1.540
$\frac{B(E2;2_2^+\rightarrow 2^+)}{B(E2;2_2^+\rightarrow 0^+)}$	120	82.9 (47)	∞	20.42 $\gamma = 25^\circ$	105
$\frac{B(E2;2_2^+\rightarrow 2^+)}{B(E2;2_2^+\rightarrow 0^+)}$	122	102 (11)		82.60 $\gamma = 27.5^\circ$	102
$\frac{B(E2;2_2^+\rightarrow 2^+)}{B(E2;2_2^+\rightarrow 0^+)}$	124	154 (35)			146
$B(E2; 0_{g.s.}^+ \rightarrow 2_1^+)$	120	0.666 (20)			
$B(E2; 0_{g.s.}^+ \rightarrow 2_1^+)$	122	0.660 (6)			
$B(E2; 0_{g.s.}^+ \rightarrow 2_1^+)$	124	0.567 (5)			

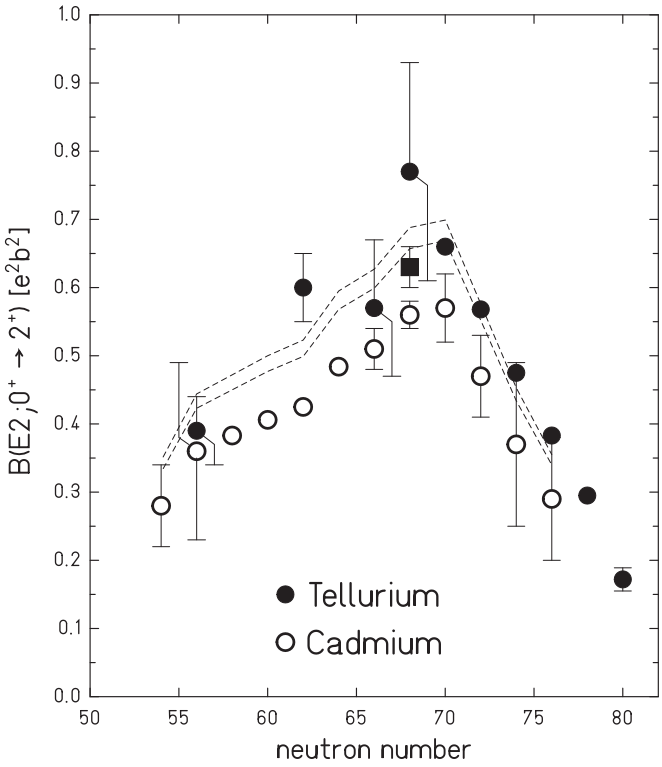

FIG. 4. Reduced transition probabilities $B(E2; 0^+_{\text{g.s.}} \rightarrow 2^+_1)$ for tellurium [14,17], along with the present result for ^{120}Te (full square symbol) and cadmium [14] isotopic chains versus the neutron number. The dashed curve is calculated from the experimental Cd data, scaled by a factor of $(52/48)^2$ in order to obtain the corresponding $B(E2; 0^+_{\text{g.s.}} \rightarrow 2^+_1)$ values in Te isotopes.

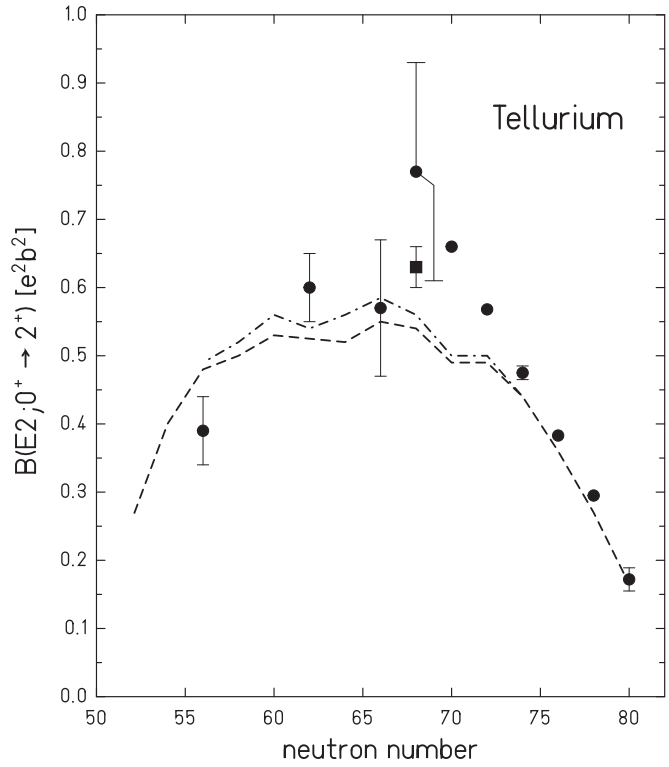

FIG. 5. Reduced transition probabilities $B(E2; 0^+_{\text{g.s.}} \rightarrow 2^+_1)$ for tellurium [14,17] isotopes with the present, more precise experimental result for ^{120}Te (full square symbol). The dashed curve (SM_a) corresponds to single-particle energies according to Ref. [5]. For the dash-dotted curve (SM_b) the $d_{5/2}$, $g_{7/2}$ orbitals were inverted (for details see text).

number is well explained by the rotational model which defines the reduced transition probability by

$$B(E2; 0^+_{\text{g.s.}} \rightarrow 2^+_1) = \left[\frac{3ZeR_o^2}{4\pi}\right]^2 \beta^2.$$

Here, $Z^2A^{4/3}$ yields the dependence on the element and mass number, respectively. While the mass difference between corresponding isotopes is rather small, the dependence on the element number for Te ($Z = 52$) and Cd ($Z = 48$) yields a ratio of $(52/48)^2$. The dashed curve in Fig. 4 is calculated from the Cd data multiplied by $(52/48)^2$ to obtain the $B(E2\uparrow)$ value of a Te isotope with the same neutron number. One obtains the same dependence on the neutron number for the Te and Cd isotopic chain. Figure 4 clearly demonstrates the need for more precise data.

In Fig. 5 the measured $B(E2; 0^+_{\text{g.s.}} \rightarrow 2^+_1)$ values for ^{120,122,124}Te isotopes and the published data [14] for other Te isotopes are also compared with predictions of LSSM calculations [17] for Te isotopes. For $N, Z = 50$ the shell closure is complex and even the relative ordering of the $g_{7/2}$ and $d_{5/2}$ orbitals has been actively debated. Therefore the calculations for tellurium isotopes were performed with two sets of single-particle energies, ϵ_{sp}. In the first set (SM_a), the values for ϵ_{sp} are identical to the tin calculation [5]. In the second set (SM_b), the new result in Ref. [18] was taken into account by setting $\epsilon_{sp}(g_{7/2}) = 0$ and $\epsilon_{sp}(d_{5/2}) = 172$ keV. With the effective charge of $e_{\nu\ \text{eff}} = 0.8$e and $e_{\pi\ \text{eff}} = 1.5$e the LSSM predictions in the model space $g_{7/2}$, $d_{5/2}$, $d_{3/2}$, $s_{1/2}$, $h_{11/2}$ reproduce the experimental $B(E2\uparrow)$ values quite well. For midshell nuclei, the model space was limited, allowing excitations of up to four neutrons in the $h_{11/2}$ subshell. This leads to an underestimation in the model predictions visible around midshell. The observed asymmetric distribution (Fig. 4) is not reproduced and requires additional theoretical interpretation.

The nuclear structure of ^{120,122,124}Te can be determined from our measured absolute $B(E2\uparrow)$ values to higher-lying states. These $B(E2)$ values, normalized to the $B(E2; 0^+_{\text{g.s.}} \rightarrow 2^+_1)$ value, are compared in Table II with the vibrational and asymmetric rotor model. In particular, the decay from the second 2^+ state allows the determination of the γ-asymmetry parameter which is close to 25° and 27.5°. For transition ratios between yrast states, e.g.,

$$\frac{B(E2; 4^+ \rightarrow 2^+)}{B(E2; 2^+ \rightarrow 0^+)},$$

one is rather insensitive to the γ degree of freedom, but the experimental data never reach the vibrational limit. Based on all experimental findings for ^{120,122,124}Te, level schemes, static

quadrupole moments, and reduced transition probabilities, one obtains the best agreement with an asymmetric-rotor behavior.

In addition, properties of ^{120,122,124}Te are also investigated in the framework of the interacting boson approximation (IBA-2), including the neutron-proton degree of freedom. The computer code NPBOS [19] was used to diagonalize the Hamiltonian. The Hamiltonian in the IBA-2 formalism is expressed as

$$H = \epsilon(n_{d\pi} + n_{d\nu}) + \kappa Q_\pi \cdot Q_\nu + \lambda M_{\pi\nu}.$$

The main part of the Hamiltonian, which determines the excitation energies of the low-lying states consists of two terms: (i) the single-d-boson energy (ϵ), and (ii) the strength and shape of the quadrupole-quadrupole interaction between neutron and proton bosons (determined by the parameter κ, χ_ν, and χ_π). Since in an isotopic chain χ_π ($\sim$−1.0) is kept constant and the parameters ϵ ($\sim$0.87) and κ ($\sim$−0.22) vary very little, the characteristic changes in one series of isotopes are described mainly by the variation of only one parameter, χ_ν ($\sim$0.8). The fitted parameters for ^{120,122,124}Te are given in brackets. The parameter χ_ν was found to be constant. In order to obtain the $O(6)$ limit of the Hamiltonian, the complete elimination of the one-d-boson changing terms, i.e., $\chi_\nu = \chi_\pi = 0$, is required. As it is pointed out by Bijker *et al.* [20], the less stringent condition $\chi_\nu = -\chi_\pi$ also leads to spectra that have many of the $O(6)$ features and in addition avoids some of the predictions of the pure $O(6)$ limit, which do not agree with experiment, such as vanishing quadrupole moments. In calculating absolute $B(E2)$ values the boson effective charges were fit to the experimental reduced transition probability $B(E2; 2_1^+ \rightarrow 0_{g.s.}^+)$. The values of the boson effective charges for all isotopes obtained are $e_\nu = 0.105$ eb and $e_\pi = 0.0955$ eb for ^{120}Te, $e_\nu = 0.116$ eb and $e_\pi = 0.0955$ eb for ^{122}Te, and $e_\nu = 0.12$ eb and $e_\pi = 0.0955$ eb for ^{124}Te. The performed IBA-2 calculations, which are close to the $O(6)$ limit, can explain the energy spectra as well as the measured $E2$ transition probabilities. It is also capable of explaining the observed nonvanishing static quadrupole moments of the first 2^+state.

In summary, several reduced transition probabilities have been measured for ^{120,122,124}Te isotopes. From the new and very precise $B(E2; 0_{g.s.}^+ \rightarrow 2_1^+)$ values the collectivity of the tellurium isotopes were determined and compared with predictions of LSSM calculations. The agreement is quite well, although the observed asymmetric distribution between $N = 50$ and $N = 82$ in Te as well as in Cd was not reproduced and requires additional theoretical interpretations. From the $B(E2\uparrow)$ values connecting higher-lying states, the nuclear structure of the ^{120,122,124}Te isotopes was determined, which shows the behavior of a soft triaxial nucleus. It clearly demonstrates that many experimental observables are needed to obtain the correct answer of the nuclear behavior.

ACKNOWLEDGMENTS

The authors would like to thank the operating staff of the IUAC accelerator for supplying an excellent Ni beam. The authors also acknowledge the GDA group for their help and support. One of the authors (M.S.) would like to thank J.B. Gupta for the many fruitful discussions. This work was performed under IUAC-GSI collaboration.

[1] I. Talmi, Nucl. Phys. A **172**, 1 (1971).
[2] http://www.nndc.bnl.gov/ensdf.
[3] A. Bockisch and A. M. Kleinfeld, Nucl. Phys. A **261**, 498 (1976).
[4] J. Barrette, M. Barrette, R. Haroutunian, G. Lamoureux, and S. Monaro, Phys. Rev. C **10**, 1166 (1974).
[5] A. Banu *et al.*, Phys. Rev. C **72**, 061305(R) (2005).
[6] T. Otsuka, Nucl. Phys. A **557**, 531 (1993).
[7] P. O. Hess, M. Seiwert, J. Maruhn, and W. Greiner, Z. Phys. A: At. Nucl. **296**, 147 (1980).
[8] K. Heyde and P. J. Brussaard, Nucl. Phys. A **104**, 81 (1967).
[9] E. Degrick and G. Vanden Berghe, Nucl. Phys. A **231**, 141 (1974).
[10] J. R. Vanhoy *et al.*, Phys. Rev. C **68**, 034315 (2003).
[11] http://www.srim.org.
[12] R. Kumar *et al.*, Phys. Rev. C **81**, 024306 (2010).
[13] A. Winther and J. de Boer, in *Coulomb Excitation*, edited by K. Alder and A. Winther (Academic Press, New York, London, 1966).
[14] S. Raman, C. W. Nestor, and P. Tikkanen, At. Data Nucl. Data Tables **78**, 1 (2001).
[15] R. Devi and S. K. Khosa, Z. Phys. A: Hadrons Nucl. **354**, 45 (1996).
[16] A. Goswami and L. Lin, Phys. Lett. B **42**, 310 (1972).
[17] T. Bäck, C. Qi, B. Cederwall, R. Liotta, F. Ghazi Moradi, A. Johnson, R. Wyss, and R. Wadsworth, Phys. Scr. **T150**, 014003 (2012).
[18] I. Darby *et al.*, Phys. Rev. Lett. **105**, 162502 (2010).
[19] T. Otsuka and N. Yoshida, The IBM-2 computer program NPBOS, University of Tokyo, 1985.
[20] R. Bijker, A. E. L. Dieperink, and O. Scholten, Nucl. Phys. A **344**, 207 (1980).